# Using Modified Time-Frequency Algorithms for Retinal Vessel Detection to Diagnose Eye Diseases

Akram Asghari Govar[1]*, Ali BaibourdiAghdam
[1]Department of Electrical Engineering, AH.C.,Islamic Azad University,Ahar,Iran
Department of Biomedical Engineering, ,AH.C.,Islamic Azad University,Ahar,Iran
[1]Email:AK-Asghari@iau.ac.ir(corresponding author)
Receive Date: 28 May 2025 Revise Date: 12 June 2025 Accept Date: 24 June 2025

## Abstract

*In medical sciences, detecting blood vessels in retinal images provides important information for ophthalmologists. The detection of vessels in retinal images is highly significant due to their critical role in eye health evaluation. These vessels are essential for diagnosing diseases, monitoring changes over time, and assessing conditions such as diabetic retinopathy, retinal artery occlusion, and ocular hypertension. To this end, this paper proposes a new algorithm for retinal vessel segmentation. The algorithm utilizes various image processing techniques, especially morphological processing. The innovative aspects of this research include using grayscale images obtained from all three channels of the color image, combining multiple images processing methods, applying Gabor filtering, and proposing a sharpening technique to enhance edges. Additionally, a modified method for background estimation and removal, as well as the use of morphological reconstruction for the final reconstruction and extraction of retinal vessels, are among the research objectives. The efficiency of the proposed algorithms has been evaluated in terms of accuracy, sensitivity, and specificity on the DRIVE and STARE datasets, and the results have been analyzed.*

**Keywords**: retinal vessels, eye diseases, Gabor filter, sharpening algorithm, image processing.

## 1. Introduction

Retinal vessel segmentation techniques are employed for screening and diagnosing cardiovascular and ocular diseases. However, only a limited number of algorithms perform well on noisy and damaged retinal images. Most techniques reported in the literature have been evaluated on a small set of images, specifically 20 images from the DRIVE database. Retinal image segmentation algorithms are broadly classified into seven main categories [1]:

1. Pattern recognition techniques
2. Matched filter techniques
3. Vessel tracking methods
4. Mathematical approaches
5. Multi-scale methods
6. Model-based approaches
7. Hardware-based/parallel techniques

In 2007, Mr. Salem and colleagues proposed a radius-based clustering algorithm (RACAL), which used a distance metric to distribute image pixels into clusters without supervision [2]. Bayesian analysis by Mr. Aurangzeb and colleagues was used for retinal vessel segmentation [3]. The concept of using guided filters to enhance retinal vessels was developed by Mr. W. T. Freeman and Z. H. Nasiruddin [4],[5]. Subsequently, Alloway and colleagues [6] improved the matched filter technique initially developed by Mr. A. Desianiwith utilizing a comprehensive and precise search optimizer function to find optimal parameters—such as filter size, standard deviation, and threshold—for 20 retinal images from the DRIVE database [7]. Mr. M. D. Saleh and colleagues

developed a segmentation algorithm that used CLAHE (Contrast Limited Adaptive Histogram Equalization) in the preprocessing stage to enhance vessel clarity and mean filtering to remove background noise [8]. Ultimately, this unsupervised classification algorithm succeeded in determining an appropriate threshold for final vessel segmentation. Researchers also employed a Mar model combined with morphological features of retinal blood vessels to extract vessels, as seen in reference [9]. Early indications of vascular wall changes in ocular diseases involve the appearance of pathological spots like exudates, microaneurysms, and hemorrhages, which manifest as bright yellowish spots and small red patches on the retina surface. The first algorithm for microaneurysm detection (considered one of the pathological lesions) was introduced in 1983 [10]. The latest method in this field, developed by Mahdizadeh and colleagues, was applied on color retinal images [11].

## 2. Image Morphological Processing:

Mathematical morphology is a branch of image processing used for analyzing structures and shapes within images. It employs mathematical concepts and its own specialized language to identify and describe image components like borders and small structures. Its foundation relies on repeating small patterns across the image The language of mathematical morphology is the language of sets. In mathematical morphology, sets essentially represent objects in the image.

### 2.1.Adaptive Smoothing Filter with CLAHE Histogram Adjustment

The CLAHE (Contrast Limited Adaptive Histogram Equalization) technique is an image processing method used to enhance image clarity. It employs a transformation derived from the image's histogram to redistribute the intensity values of all pixels. This approach can yield good results when the distribution of pixel intensities across the entire image is uniform. However, in areas where regions are significantly brighter or darker, the overall image clarity may not improve sufficiently. To address this issue, the Adaptive Histogram Equalization (CAHE) technique is used. This method calculates histograms for different parts of the image and uses them to redistribute the intensity or brightness values locally. As a result, this technique is effective for improving local contrast and highlighting details within images. The main idea is to analyze geometric structures by overlapping the image with small patterns—called elements—that are regarded as structural elements. The two primary morphological operations are dilation and erosion. Dilation enlarges objects, making them thicker, while erosion reduces an object, thinning it. The dilation process is controlled by the shape and size of the structuring element. Two other important morphological operations are introduced: opening and closing. Opening generally smooths object contours, softening narrow corners, and removing sharp protrusions. Closing, on the other hand, smooths the contours but tends to eliminate thin cracks and gaps, filling small holes and connecting nearby elements.

### 2.2.Morphological reconstruction

Morphological reconstruction is a process that involves two images and a structuring element (rather than just one image and a structuring element). The image that specifies the starting point of the transformation is called the marker image. The other image, which constrains the transformation, is called the mask image. The structuring element is used to define the connectivity and how the reconstruction progresses,

### 2.3.The 2D Gabor filter

The Gabor filter is among the most widely used methods for extracting texture features. It captures significant textural characteristics from images, encompassing various orientations and frequencies. When defined in the frequency domain, the Gabor filter involves applying a Fourier transform to the input image using a Gaussian function, transforming it into the frequency domain, and then multiplying it with the Gabor filter in that domain. This filter has a real part and an imaginary part, which can be used separately or combined in a single expression. The Gabor filter kernel aligns with the receptive fields of simple cells in the human visual system, resulting from the modulation of sinusoidal and Gaussian signals. Gabor energy models the behavior of complex cells in the visual system and serves as an effective feature in many tissue analysis methods.

## 3. Suggested Algorithm:

The proposed algorithm in this paper is unsupervised and is applied to grayscale retinal images. To create a grayscale image, all three channels of a color retinal image are used. Therefore, the grayscale image used contains vascular features from all three-color channels. The process begins by comparing the three-color channels of the retinal images, followed by explaining how to obtain an appropriate grayscale image for implementing the proposed retinal vessel segmentation algorithm.

### 3.1.Clarity comparison of the three retinal image channels:

A color retinal image consists of three channels: red, green, and blue. Each channel is stored in an M×N matrix, with each pixel having a value between 0 and 255. Combining these three channels produces the full-color image. The clarity of these channels in retinal images varies. The red channel has a very bright intensity distribution, while the blue channel displays darker vessel intensities. However, the green channel provides the most suitable representation for blood vessel visualization. For better understanding, Figs 1 and 2 illustrate examples from the DRIVE and STARE datasets.

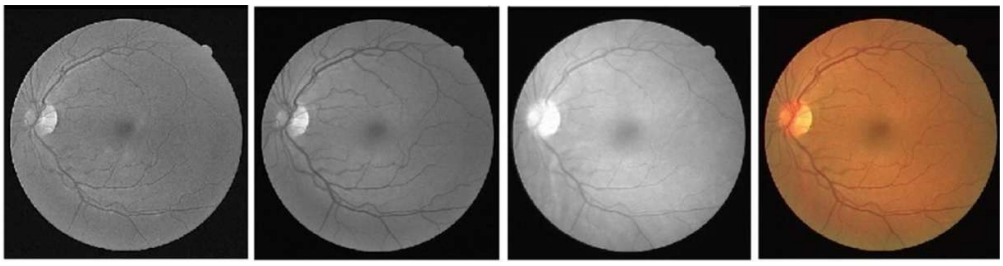

**Fig.1.**DRIVE database image: a) Original image, b) Redchannelc)Green channeld)Blue channel

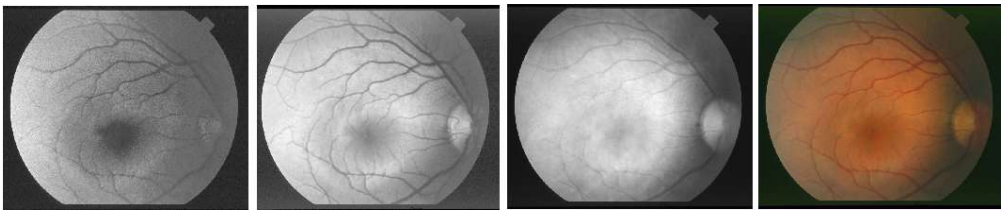

**Fig.2.**STARE database image: a)Original image,b)Red channel,c)Green channel,d)Blue channel

By using a color filter, the brightness levels of each color can be adjusted. This filter modifies the values of each matrix based on specific criteria, enhancing the target objects in the image and making them more prominent. To achieve this, the red components of the image are attenuated, as these components tend to be homogeneous in the background of the eye and blood vessels, helping to emphasize the vascular structures. The green and blue components are positioned slightly higher than the red components because they contain higher-frequency information related to the examined veins. Therefore, the red components are multiplied by a scalar value of 0.4, the green components by 2, and the blue components by 1.8. The images obtained from the previous step are used to create a grayscale image with a weighted average, composed of the three components we introduced earlier. For this purpose, the following formula is used.

$$I_{Gray} = 0.2989R + 0.5870G + 0.1140B \quad (1)$$

In the above relation, R, G, and B represent the pixels corresponding to the red, green, and blue channels, respectively. Therefore, the grayscale image obtained from the previous step is used to implement the proposed retinal vessel segmentation algorithm. Figure 3 shows, in order, the color images and the resulting grayscale image after applying the algorithm on the retinal color image.

**Fig.3.**a) Color image, b) Grayscale image

The innovations of the proposed algorithm are as follows:

- Designing a new algorithm to extract retinal blood vessels using the grayscale images obtained from each of the three colors.
- Using a combination of image processing techniques, the improved Gabor filter, and sharpening methods to enhance image clarity.
- Proposing an improved method for background removal to obtain an image with a smooth background, along with the use of morphological reconstruction techniques for the final extraction of retinal blood vessels.

Preprocessing phase:

This phase includes two sections:

1) Local enhancement of image clarity using the CLAHE technique
2) Noise reduction and image enhancement using the Gabor filter

In the first stage, the clarity of the retinal blood vessels in the grayscale image

obtained from the previous step is improved using the CLAHE technique. This technique, when combined with various image processing methods, provides very suitable results for segmentation and image processing applications. Therefore, we were able to achieve an image with better clarity using this method. In the second stage, the Gabor filter—which is essentially a two-dimensional Gaussian function—is applied. In this stage, the variance parameters of the Gaussian function along both the x and y axes were set to 1.5, and the central frequency parameters along these axes were set to 2. Additionally, the rotation angle was adjusted to 360 degrees. This choice was based on evaluating the filter response at orientations of 0°, 45°, 90°, and 360°, with the best Gabor filter response observed at 360°. Consequently, the Gabor filter was applied at 360° to the images, and the resulting image was used for subsequent steps in the algorithm. The images demonstrating the application of the CLAHE operator and Gabor filter are presented in Figure 4.

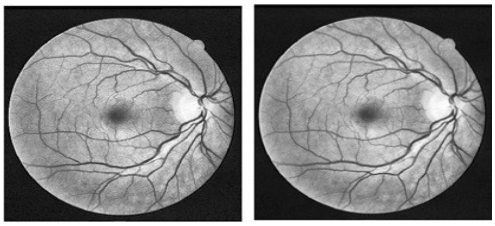

**Fig.4.**a) Image obtained after applying the CLAHE operator. b) Image obtained after applying the Gabor filter.

### 3.2.Processing phase:

To sharpen the edges of vessels and further enhance them in retinal images, we propose a method to make the image sharper and improve the visibility of existing edges. These edges mainly correspond to thin and thick vessels in the retina. For this purpose, we suggest a sharpening mask. This mask is essentially a 3×3 filter that uses the Laplacian of Gaussian filter to obtain an image with prominent edges, applied to each pixel of the image. In this filter, a parameter called alpha is used to highlight the vessel edges in the image. The alpha parameter controls the shape of the Laplacian function and should be a value between zero and one. This parameter adjusts the sharpening strength of the image edges and was set to a moderate value in the proposed algorithm. The main advantage of this method is its simplicity of implementation. Moreover, this sharpening filter is an effective method for highlighting element edges in images without causing an increase in noise pixels. The overall structure of the sharpening filter and the proposed filter can be observed in Figure 1-5, parts a and b, respectively.

$$\frac{1}{(\alpha+1)}\begin{bmatrix} -\alpha & \alpha-1 & -\alpha \\ \alpha-1 & \alpha+5 & \alpha-1 \\ -\alpha & \alpha-1 & -\alpha \end{bmatrix} \quad (2)$$

$$\frac{1}{2}\begin{bmatrix} -1 & 0 & -1 \\ 0 & 6 & 0 \\ -1 & 0 & -1 \end{bmatrix} \quad (3)$$

An example of applying the proposed filter to an image is shown in Figure5. As observed, the unclear edges in the image are effectively sharpened and emphasized, resulting in clearer and more prominent vessel boundaries.

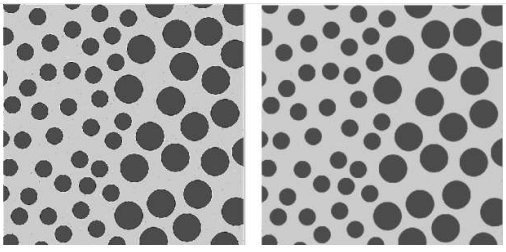

**Fig.5.** a) original image b) Sharpened image

At this stage, we propose an improved method for estimating an appropriate background image. This modified approach utilizes the median filter. The median filter has the following features:

- It effectively reduces impulse noise.
- It preserves edge information in the image.
- It prevents the creation of unrealistic intensity values for a pixel, since the median pixel value is derived from the actual intensities.

In the conventional method, a smoothed and blurred image of the original is first obtained to estimate the background. Then, this background estimate is subtracted from the original image. As a result, a final image with a smooth and reduced background is obtained. However, this method has a drawback because, after subtracting the background, dark and light regions appear in the image. These areas negatively affect the results of subsequent processing steps. To this end, by adding an additional step to the background estimation process of the images, we were able to achieve a more suitable image in terms of background smoothness. To this end, we first apply a median filter with a large size to the image, and then perform a minimization step between the resulting image and the original image. This process ensures that pixels with sharp intensities and narrow widths, which are scattered like noise in the image, are included in the calculated background. By reducing these from the original image, we can achieve a smoother image. The mathematical concept of this method can be expressed as the following equation:

$$g_{enhanced}(x,y) = f(x,y) - \min(f(x,y), h_{median}(x,y)) \quad (4)$$

In the above expression, f is the original image, h is the image obtained after applying the median filter, and g is the resulting smoothed background image. In the proposed method, the median filter size is set to a large value of 30. Then, a minimization operation is performed between the obtained image and the original image, and finally, the resulting image is subtracted from the original image. Thus, a uniform background image is obtained. In this stage, a sharpening filter is used to highlight the edges of the vessels, then, employing the modified background subtraction method, an estimate of the background is obtained using the median filter. This estimated background is then subtracted from the previous image. The images resulting from the application of the sharpening filter and the background subtraction process can be seen in Figure6.

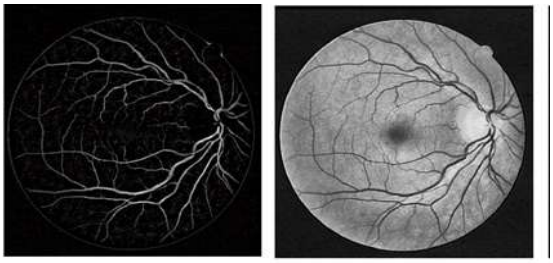

**Fig.6.** a) Image after applying the sharpening filter b) Image with a smooth background

### 3.3.Post-processing phase:

Here, the type of connectivity used for the morphological reconstruction of the vessel structure is four-connectivity. This means there is a path with four-connectivity between the two target pixels. In Figure7, you can see examples of four-connectivity and eight-connectivity.

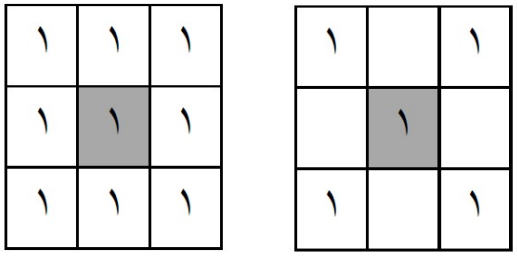

**Fig.7.**:a) Four-connectivity, b) Eight-connectivity

In the post-processing stage, morphological reconstruction is used to rebuild the vessel regions, eliminate non-vessel pixels remaining in the image, and obtain a binary image where the vessel intensities are at their maximum and the background intensities are at their minimum. The two images needed to perform this operation are the mask image and the marker image. The reconstructed image, after removing the circle around the eye, results in an appropriate binary image showing both thin and thick vessels from the retinal images. To remove the circle around the eye, we proceed as follows: based on the histogram of the retinal image, a threshold value is selected such that the entire retina is distinguished as a separate object from the image border.

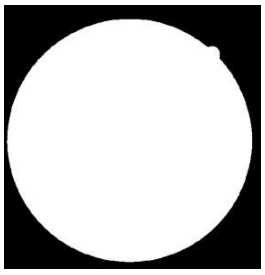

**Fig.8.** Retinal image as a separate object from the entire image

Here, the retinal pixels have the maximum value of 255, while other points have a value of zero.

If this image is multiplied pixel-by-pixel with the final vessel extraction image, the pixels corresponding to zero will become zero, while those multiplied by 255 will retain their original values. This effectively isolates the retinal area by hiding everything outside it. To remove the retina boundary, the image obtained in Figure8 is first eroded using an erosion operator with a small structuring element, which in this case is considered to be 2 pixels in size. Thus, when the eroded image is overlaid on the final vessel extraction image, the edge pixels around the retina with zero value are covered. Therefore, after multiplying the two images, the circle around the retina is removed. At this stage, the image obtained from the previous step is converted into a binary image using morphological reconstruction techniques. The marker image is obtained by applying a large value as the threshold value. The mask image is obtained by applying a small value as the threshold value .Selecting an appropriate threshold value for obtaining the mask and marker images is done through trial and error. First, using the resolution matching tool in MATLAB simulation software, we determine an appropriate threshold at which the maximum number of retinal vessel pixels are observed with the fewest non-vessel pixels in the image.

This threshold value should be large enough to provide the marker image, which includes the initial points for growth. Then, the second threshold is selected so that the maximum number of retinal vessel pixels can be visible regardless of the number of non-vessel pixels in the image. Afterwards, by applying the morphological reconstruction operator and observing the resulting image, the thresholds are updated and adjusted through trial and error to achieve an image that contains the maximum vessel pixels and the minimum

non-vessel pixels in the final reconstructed image. The images related to the marker, mask, and reconstructed image are visible in Figure9.

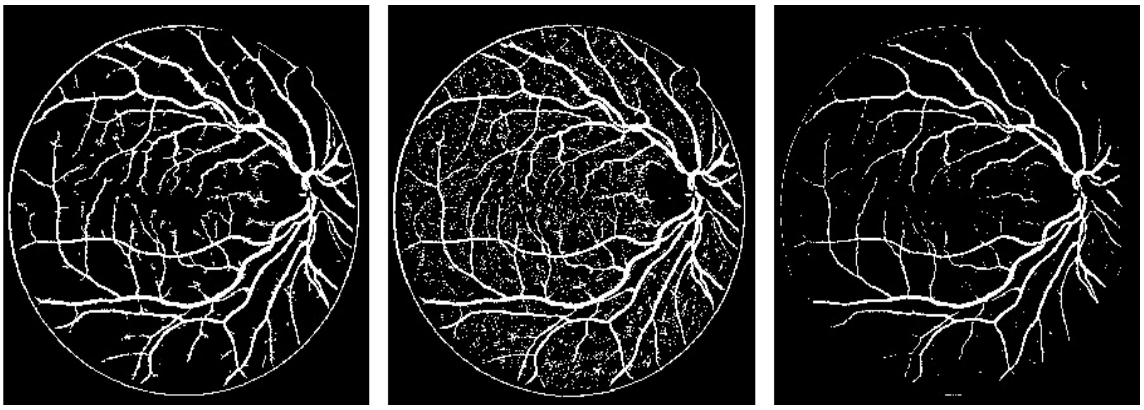

**Fig.9.** a) Marker Image, b) Mask Image, c) Reconstructed Image

### 3.4.Samples of the final segmentation images:

Samples of segmented images using the proposed algorithm after removing the circle around the retina are shown on the DRIVE and STARE databases, respectively, in Figures 10 and 11.

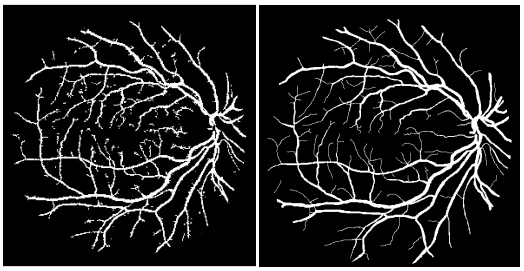

**Fig.10.** sample images DRIVE, a) standard image, b) image segmented by the proposed algorithm.

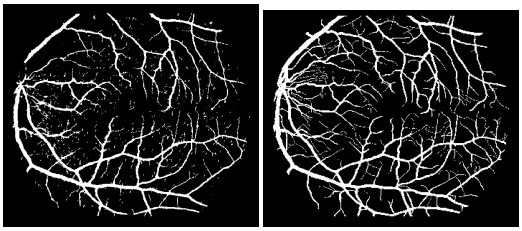

**Fig.11.** sample images STARE, a) standard image, b) image segmented by the proposed algorithm

The proposed algorithm has been applied to all images in the DRIVE and STARE databases, and the evaluation metrics—accuracy, sensitivity, and specificity—were calculated for each image. Then, the average values for each metric were obtained. Table1 presents the evaluation results of the proposed algorithm on 40 images from the DRIVE database. Table 2 shows the evaluation results on 20 images from the STARE database.

## 4. Comparison of the proposed algorithm with other approaches:

Tables 3 and 4 compare the proposed algorithm with other retinal vessel segmentation methods. Since the ultimate goal is to improve accuracy, sensitivity, and specificity, the proposed method is evaluated against the other techniques listed in these tables.

**Table1.** The values obtained from the implementation of the proposed algorithm for the DRIVE database.

| Figure number | accuracy | specificity | sensitivity |
|---|---|---|---|
| 1 | 0.9606 | 0.9771 | 0.7921 |
| 2 | 0.9536 | 0.9705 | 0.8054 |
| 3 | 0.9410 | 0.9619 | 0.7521 |
| 4 | 0.9614 | 0.9906 | 0.6725 |
| 5 | 0.9595 | 0.9890 | 0.6735 |
| 6 | 0.9557 | 0.9881 | 0.6549 |
| 7 | 0.9489 | 0.9731 | 0.7083 |
| 8 | 0.9491 | 0.9724 | 0.7008 |
| 9 | 0.9595 | 0.9835 | 0.6864 |
| 10 | 0.9613 | 0.9848 | 0.6989 |
| 11 | 0.9502 | 0.9741 | 0.7076 |
| 12 | 0.9515 | 0.9684 | 0.7730 |
| 13 | 0.9493 | 0.9719 | 0.7408 |
| 14 | 0.9514 | 0.9650 | 0.7959 |
| 15 | 0.9592 | 0.9746 | 0.7593 |
| 16 | 0.9583 | 0.9734 | 0.8068 |
| 17 | 0.9526 | 0.9735 | 0.7268 |
| 18 | 0.9553 | 0.9666 | 0.8240 |
| 19 | 0.9686 | 0.9800 | 0.8426 |
| 20 | 0.9654 | 0.9826 | 0.7492 |
| 21 | 0.9557 | 0.9677 | 0.8069 |
| 22 | 0.9583 | 0.9828 | 0.7114 |
| 23 | 0.9276 | 0.9422 | 0.7193 |
| 24 | 0.9532 | 0.9879 | 0.6882 |
| 25 | 0.9492 | 0.9915 | 0.5513 |
| 26 | 0.9481 | 0.9660 | 0.7518 |
| 27 | 0.9587 | 0.9837 | 0.7000 |
| 28 | 0.9461 | 0.9672 | 0.7509 |
| 29 | 0.9520 | 0.9709 | 0.7453 |
| 30 | 0.9509 | 0.9683 | 0.7465 |
| 31 | 0.9541 | 0.9701 | 0.7055 |
| 32 | 0.9561 | 0.9741 | 0.7543 |
| 33 | 0.9453 | 0.9596 | 0.7836 |
| 34 | 0.8899 | 0.9138 | 0.6697 |
| 35 | 0.9621 | 0.9807 | 0.7658 |
| 36 | 0.9512 | 0.9823 | 0.6965 |
| 37 | 0.9518 | 0.9709 | 0.7521 |
| 38 | 0.9503 | 0.9635 | 0.8084 |
| 39 | 0.9529 | 0.9665 | 0.8074 |
| 40 | 0.9601 | 0.9719 | 0.8168 |
| Average | 0.9521 | 0.9726 | 0.7400 |

**Table 2**. The values obtained from the implementation of the proposed algorithm for the STARE database

| Figure number | accuracy | specificity | sensitivity |
|---|---|---|---|
| 1 | 0.9291 | 0.9423 | 0.7768 |
| 2 | 0.9495 | 0.9731 | 0.6187 |
| 3 | 0.9324 | 0.9417 | 0.7854 |
| 4 | 0.9544 | 0.9887 | 0.5259 |
| 5 | 0.9440 | 0.9652 | 0.7307 |
| 44 | 0.9543 | 0.9738 | 0.6948 |
| 77 | 0.9446 | 0.9519 | 0.8606 |
| 81 | 0.9477 | 0.9574 | 0.8264 |
| 82 | 0.9525 | 0.9636 | 0.8223 |
| 139 | 0.9226 | 0.9284 | 0.8556 |
| 162 | 0.9657 | 0.9751 | 0.8434 |
| 163 | 0.9616 | 0.9743 | 0.8905 |
| 235 | 0.9581 | 0.9780 | 0.7543 |
| 236 | 0.9549 | 0.9733 | 0.7704 |
| 239 | 0.9491 | 0.9787 | 0.6363 |
| 240 | 0.9446 | 0.9753 | 0.6744 |
| 255 | 0.9620 | 0.9755 | 0.8253 |
| 291 | 0.9727 | 0.9924 | 0.6043 |
| 319 | 0.9698 | 0.9871 | 0.5849 |
| 324 | 0.9534 | 0.9792 | 0.5924 |
| Average | 0.9511 | 0.9688 | 0.7337 |

**Table 3.** Comparison of the proposed algorithm with previous methods described in the papers on the DRIVE database.

| method | accuracy | sensitivity | specificity |
|---|---|---|---|
| proposed method | 95.21 | 74.00 | 97.26 |
| Ricci [12] | 95.63 | - | - |
| Osareh [13] | 95.24 | 96.14 | 94.84 |
| Lili Xu[14] | 93.28 | 77.60 | _ |
| Nilanjan Dey[16] | 95.03 | 99.62 | 54.66 |
| Fraz [17] | 95.79 | 75.02 | 85.97 |
| BaishengDai[18] | 94.60 | 70.91 | 98.06 |
| Lupascu [20] | 95.97 | - | - |
| Li [19] | - | 78.00 | 80.97 |

**Table 4.** Comparison of the proposed algorithm with previous methods described in the articles on the STARE database.

| method | accuracy | sensitivity | specificity |
|---|---|---|---|
| proposed method | 95.11 | 73.37 | 96.88 |
| Ricci[12] | 95.84 | - | - |
| Diego Marin [15] | 95.26 | 69.44 | 98.19 |
| [2]Salem | - | 82.15 | 97.50 |
| Fraz [17] | 94.42 | 73.11 | 96.80 |
| [19]Li | - | 75.20 | 98.00 |
| [21]Lam | 96.14 | - | - |

## 5. Conclusion

To evaluate the proposed method, accessible datasets DRIVE and STARE were utilized, which include both diseased and healthy retinal images, along with standard manually segmented images. Ultimately, the evaluation metrics of accuracy, sensitivity, and specificity for the proposed algorithm on the DRIVE dataset were 95.21%, 74.00%, and 97.26%, respectively. On the STARE dataset, these values were 95.11%,73.37%, and 96.88%. The results of evaluating the proposed algorithm demonstrate that it can effectively perform retinal vessel segmentation, providing clinicians with accurate and reliable information about retinal blood vessels. Another advantage of the proposed algorithm is its ability to extract both thin and thick blood vessels, which helps clinicians accelerate the diagnosis and monitoring of eye diseases. Additionally, it eliminates the need for expert personnel to manually segment retinal vessels, a task that is time-consuming and requires high precision and concentration. Furthermore, this allows for remote patient examinations and the efficient analysis of large volumes of retinal images from many patients, significantly reducing processing time. Since the retinal vascular tree varies from person to person, one potential application of the proposed algorithms is biometric identification, leveraging individual vascular patterns for recognizing individuals. Additionally, the proposed algorithms can be utilized for various applications such as segmentation, early disease detection, and screening efforts. On the other hand, since the proposed algorithms are executed by a computer, they produce consistent results. Segmentation of the retinal blood vessels by experts, in addition to being costly and time-consuming, can vary in results depending on the individual specialist. This variation is due to fatigue caused by concentration, resulting from the high sensitivity of manual image segmentation, which leads to discrepancies in the images obtained by different experts. Therefore, using the proposed algorithms, considering the favorable evaluation metrics and their capability in extracting retinal blood vessels, is always cost-effective. This is because the outcome of retinal vessel segmentation using these algorithms will be consistent regardless of where they are applied in the world.

## References

[1] M. M. Fraz, P. Remagnino, A. Hoppe, B. Uyyanonvara, A. R. Rudnicka, C. G. Owen, et al., "Blood vessel segmentation methodologies in retinal images–A survey," Computer methods and programs in biomedicine, vol. 108, pp. 407-433, 2012.

[2] S. A. Salem, N. M. Salem, and A. K. Nandi, "Segmentation of retinal blood vessels using a novel clustering algorithm (RACAL) with a partial supervision strategy," Medical & biological engineering & computing, vol. 45, pp. 261-273, 2007.

[3] K. Aurangzeb, R. S. Alharthi, S. I. Haider and M. Alhussein, "An Efficient and Light Weight Deep Learning Model for Accurate Retinal Vessels Segmentation," in IEEE Access, vol. 11, pp. 23107-23118, 2023.

[4] W. T. Freeman and E. H. Adelson, "The design and use of steerable filters," IEEE Transactions on Pattern analysis and machine intelligence, vol. 13, pp. 891-906, 1991.

[5] Z. H. Nasiruddin, W. M. Diyana W Zaki, S. A. Hudaibah and A. H. Nur Asyiqin, "Automated Retinal Blood Vessel Feature Extraction in Digital Fundus Images," 2022 IEEE International Conference on Artificial Intelligence in Engineering and Technology (IICAIET), Kota Kinabalu, Malaysia, 2022.

[6] M. Al-Rawi, M. Qutaishat, and M. Arrar, "An improved matched filter for blood vessel detection of digital retinal images," Computers in Biology and Medicine, vol. 37, pp. 262-267, 2007.

[7] A. Desiani, Erwin, B. Suprihatin, F. Efriliyanti, M. Arhami and E. Setyaningsih, "VG-DropDNet a Robust Architecture for Blood Vessels Segmentation on Retinal Image," in IEEE Access, vol. 10, pp. 92067-92083, 2022.

[8] M. D. Saleh, C. Eswaran, and A. Mueen, "An automated blood vessel segmentation algorithm using histogram equalization and automatic threshold selection," Journal of Digital Imaging, vol. 24, pp. 564-572, 2011.

[9] L. Espona, M. J. Carreira, M. Ortega, and M. G. Penedo, "A snake for retinal vessel segmentation," in Pattern Recognition and Image Analysis, ed: Springer, 2007, pp. 178-185.

[10] Walter T, Massin P, Ali Erginay A, Ordonez R ,Jeulin C, Klein JC, "Automatic detection of microaneurysms in color fundus images," Med Image Analysis,11: 555–66, 2007.

[11] Porreza HR, Bahreyni Toossi MH, Mehdizadeh AR, Pourreza R, Tavakoli M, "Automated detection of microaneurysm in color fundus by using local radon transform," Iranian Journal of Medical Physics, 6(1):1320, 2009.

[12] E. Ricci and R. Perfetti, "Retinal blood vessel segmentation using line operators and support vector classification," Medical Imaging, IEEE Transactions on, vol. 26, pp. 1357-1365, 2007.

[13] A. Osareh and B. Shadgar, "Automatic blood vessel segmentation in color images of retina," Iran. J. Sci. Technol. Trans. B: Engineering, vol. 33, pp. 191-206, 2009.

[14] L. Xu and S. Luo, "A novel method for blood vessel detection from retinal images," Biomedical engineering online, vol. 9, p. 14, 2010.

[15] D. Marín, A. Aquino, M. E. Gegúndez-Arias, and J. M. Bravo, "A new supervised method for blood vessel segmentation in retinal images by using gray-level and moment invariants-based features," Medical Imaging, IEEE Transactions on, vol. 30, pp. 146-158, 2011.

[16] N. Dey, A. B. Roy, M. Pal, and A. Das, "FCM Based Blood Vessel Segmentation Method for Retinal Images," arXiv preprint arXiv:1209.1181, 2012.

[17] M. M. Fraz, S. Barman, P. Remagnino, A. Hoppe, A. Basit, B. Uyyanonvara, et al., "An approach to localize the retinal blood vessels using bit planes and centerline detection," Computer methods and programs in biomedicine, vol. 108, pp. 600-616, 2012.

[18] B. Dai, W. Bu, X. Wu, and Y. Teng, "Retinal vessel segmentation via Iterative Geodesic Time Transform," in Pattern Recognition (ICPR), 2012 21st International Conference on, 2012, pp. 561-564.

[19] Li W, Bhalerao A, Wilson R, ”Analysis of retinal vasculature using a multiresolution Hermite model”, IEEE Transactions on Medical Imaging. vol. 26, PP 137–152, 2007.

[20] Lupascu C.A, Tegolo D, Trucco E, ”FABC: retinal vessel segmentation using AdaBoost”, IEEE Transactions on Information Technology in Biomedicine, vol. 14 ,pp 1267–1274, 2010.

[21] Lam B.S.Y, Yongsheng G, Liew A.W.C, ”General retinal vessel segmentation using regularization-based multi concavity modeling”, IEEE Transactions on Medical Imaging, vol. 29 ,PP 1369–1381, 2010.